Journal of Cerebral Blood Flow and Metabolism
4:212–223 © 1984 Raven Press, New York

Regional Kinetic Constants and Cerebral Metabolic Rate for Glucose in Normal Human Volunteers Determined by Dynamic Positron Emission Tomography of [^{18}F]-2-Fluoro-2-deoxy-D-glucose

W.-D. Heiss, G. Pawlik, K. Herholz, R. Wagner, H. Göldner, and K. Wienhard

Max-Planck-Institut für Neurologische Forschung, Köln, F.R.G.

Summary: Using dynamic [^{18}F]fluorodeoxyglucose (FDG) positron emission tomography with a high-resolution, seven-slice positron camera, the kinetic constants of the original three-compartment model of Sokoloff and co-workers (1977) were determined in 43 distinct topographic brain regions of seven healthy male volunteers aged 28–38 years. Regional averages of the cerebral metabolic rate for glucose (CMR_{glu}) were calculated both from individually fitted rate constants (CMR_{glu}kinetic) and from activity maps recorded 30–40 min after FDG injection, employing a four-parameter operational equation with standard rate constants from the literature (CMR_{glu}autoradiographic). Metabolic rates and kinetic constants varied significantly among regions and subjects, but not between hemispheres. k_1 ranged between 0.0485 ± 0.00778 min^{-1} in the oval center and 0.0990 ± 0.01347 min^{-1} in the primary visual cortex. k_2 ranged from 0.1198 ± 0.01533 min^{-1} in the temporal white matter to 0.1472 ± 0.01817 min^{-1} in the cerebellar dentate nucleus. k_3 was lowest (0.0386 ± 0.01482 min^{-1}) in temporal white matter and highest (0.0823 ± 0.02552 min^{-1}) in the caudate nucleus. Maximum likelihood cluster analysis revealed four homogeneous groups of brain regions according to their respective kinetic constants: (1) white matter and mixed brainstem structures; (2) cerebellar gray matter and hippocampal formations; (3) basal ganglia and frontolateral and primary visual cortex; and (4) other cerebral cortex and thalamus. Across the entire brain, k_1 and k_2 were positively correlated (r = 0.79); k_1 and k_3 showed some correlation (r = 0.59); but no significant linear association was found between k_2 and k_3. A strong correlation with CMR_{glu} could be demonstrated for k_1 (r = 0.88) and k_3 (r = 0.90), but k_2 was loosely correlated (r = 0.56). CMR_{glu} kinetic ranged from 17.0 ± 2.45 μmol/100 g/min in the occipital white matter to 41.1 ± 5.62 μmol/100 g/min in the frontolateral cortex. In most regions the mean values of CMR_{glu} kinetic did not differ significantly from CMR_{glu} autoradiographic. With few exceptions, however, within-region variance was significantly less for CMR_{glu} kinetic than for CMR_{glu} autoradiographic, suggesting greater individual reliability of results obtained by the kinetic approach. **Key Words:** Cluster analysis—Dynamic positron emission tomography—[^{18}F]-2-Fluoro-2-deoxy-D-glucose—Normal values—Regional cerebral glucose metabolism—Regional rate constants.

Advanced multislice equipment for positron emission tomography (PET) with improved spatial resolution permits the determination of isotope concentrations in rather small brain regions. Using the [^{18}F]-2-fluoro-2-deoxy-D-glucose (FDG) method, the cerebral metabolic rate for glucose (CMR_{glu}) can be estimated (Reivich et al., 1979) in distinct anatomical structures of the central nervous system. Those computations commonly have been based on a standard lumped constant and on rate constants determined in healthy volunteers for gray and white matter regardless of regional variability. It is to be expected, though, that differences in the cytoarchitecture and function of cortex, basal ganglia, cerebellum, and brainstem are paralleled by differences in the kinetic constants for transport and metabolism characteristic of the respective structures. Therefore, estimates of metabolic rates obtained with standard rate constants derived mainly from cortical tissue and the oval center may be substantially biased, especially in deeper brain regions. Al-

Address correspondence and reprint requests to Dr. Heiss at Max-Planck-Institut für Neurologische Forschung, Ostmerheimer Str. 200, D-5000 Köln 91 (Merheim), F.R.G.

Abbreviations used: CMR_{glu}, cerebral metabolic rate for glucose; CT, computerized tomography; FDG, [^{18}F]-2-fluoro-2-deoxy-D-glucose; FWHM, full width at half-maximum; PET, positron emission tomography.

though the lumped constant has not been measured regionally in humans, the error caused by employing inappropriate standard rate constants can be minimized. It was the purpose of this study to determine individual kinetic constants in small brain regions of healthy volunteers by dynamic scanning to derive least biased estimates of CMR_{glu} for various parts of the central nervous system.

METHODS

Subjects

The study was performed on seven healthy male medical doctors aged 28–38 years, who were familiar with the examination procedure and showed only minimal tension, apprehension, or excitement. Volunteers were comfortably placed on a reclining chair in a room with low ambient light and noise, eyes closed and ears unplugged. Approximately 15 min before starting the examination, short catheters were inserted into one cubital vein for injection and into a vein of the contralateral hand that was subsequently kept in a thermostat-controlled water bath at 44°C for blood sampling as described by Phelps et al. (1979). Subjects were instructed to relax and not to move or speak during the study. All stayed awake and their plasma glucose levels, averaging 5.4 ± 0.48 mmol/L, remained stable throughout the examination.

Materials and scanning procedure

FDG of a specific activity of 10–20 mCi (370–740 MBq)/mg at the time of injection was synthesized according to the method of Ido et al. (1977) using a remote-controlled synthesis system (Barrio et al., 1981; Fowler et al., 1981). Radiochemical purity, as assessed by thin-layer chromatography, was >95%, the impurity being partly hydrolyzed protected glucopyranosylfluoride. Each subject received a rapid intravenous bolus injection of ~5 mCi FDG in 5 ml sterile, pyrogenfree, normal saline solution, and recording was started immediately. Seven equally spaced parallel planes, centered from the canthomeatal line up to 81 mm above it, were simultaneously scanned for 40 min at consecutive intervals, gradually increasing from 1 to 5 min, using a four-ring positron camera (Scanditronix PC 384) with a spatial resolution of ~8 mm full width at half-maximum (FWHM) in 11-mm slices (Eriksson et al., 1982). This procedure yielded dynamic information on tracer accumulation in virtually all major structures of the brain. During the last run, 35–40 min after FDG injection, the number of coincidence counts from the largest scanned slice was >1,300,000 in all cases. Data from the tomographic device and from a sample changer used for plasma counting, as well as plasma glucose values determined in duplicate by a standard enzymatic method, were stored in the memory of a VAX 11/780 (DEC) computer for later processing.

Image processing

The spatial activity distribution in the scanned slices was reconstructed employing: (1) an edge-finding algorithm to determine the skull contour for attenuation correction (Bergström et al., 1982); (2) a deconvolution for subtraction of scattered radiation (Bergström et al., 1983); and (3) a filtered backprojection algorithm. This resulted in a 128 × 128 matrix that was displayed as an interpolated 256 × 256 pixel image. Activities measured in tissue and in plasma were corrected for decay and adjusted by cross-calibration of the respective counters.

On each tomographic image an average of 15 regions of interest was outlined, representing distinct anatomical structures according to standard neuroanatomical and computerized tomography (CT) atlases (Matsui and Hirano, 1978) and individual X-ray CT scans. Cortical regions were largely contiguous, but great care was taken to keep the bias caused by partial volume effect at the borders between white and gray matter, or cerebrospinal fluid space, at a minimum. Larger topographic units were formed by lumping matching regions of interest from different slices. The model equation described by Sokoloff et al. (1977) was fitted to the time-activity data sequentially sampled within each of those regions, utilizing an advanced system for fast function minimization (James and Roos, 1976). In this fit procedure, only the tomographic information obtained after the third minute, i.e., after plasma concentration had dropped below tissue level (see Fig. 2), was used to exclude influences of bolus shape. In view of the small proportion of intracerebral vascular volume and the comparatively low plasma FDG concentration after the fourth minute, background activity in the tissue was considered negligible. Because measuring time was restricted to 40 min after FDG injection, no attempt was made to determine the dephosphorylation rate constant, k_4 (Phelps et al., 1979). In addition to the dynamic approach, regional activities recorded 30–40 min after FDG injection were used to compute metabolic rates (CMR_{glu} autoradiographic) according to the *in vivo* autoradiographic method employing a four-parameter operational equation with standard rate constants (Phelps et al., 1979).

Mathematical model

The Sokoloff model assumes three distinct compartments: FDG in plasma, tissue pool of free FDG, and FDG-6-phosphate trapped in the tissue. The temporal distribution of the regional tissue activity of ^{18}F, C_i^*, and the plasma FDG concentration as a function of time, C_p^*, are related by the rate constants k_1, k_2, and k_3, describing the kinetics of regional FDG turnover:

$$C_i^*(\tau) = [k_1k_3/(k_2 + k_3)]\left\{\int_0^\tau C_p^*(t)dt - \exp[-(k_2 + k_3)\tau]\int_0^\tau C_p^*(t)\exp[(k_2 + k_3)t]dt\right\}$$

$$+ k_1\exp[-(k_2 + k_3)\tau]\int_0^\tau C_p^*(t)\exp[(k_2 + k_3)t]dt \quad (1)$$

In this operational equation the individual rate constants represent the transport of FDG from plasma to brain tissue (k_1), back from tissue to plasma (k_2), and FDG phosphorylation in the tissue (k_3). Once the regional set of kinetic constants is known, the corresponding metabolic rate for glucose can be calculated according to

$$CMR_{glu}kinetic = \frac{C_p}{LC} \times \frac{k_1 k_3}{k_2 + k_3} \quad (2)$$

where C_p denotes plasma glucose concentration. In the present series an estimated average value of 0.42 (Huang et al., 1980) was used for the lumped constant, LC, to correct for differences in the behavior of glucose and FDG with respect to transport and phosphorylation.

Statistical analysis

Reported averages represent the arithmetic mean ± SD or, when indicated, the coefficient of variation. Rate constants as well as metabolic rates in all topographic regions, consisting of up to five contiguous regions of interest from various slices, were compared by means of factorial analyses of variance with regard to differences between corresponding regions on either hemisphere, among subjects and regions, and between methods of determing CMR_{glu}. Relative variance components were estimated following standard procedures applicable to mixed models, and tests of significance were performed according to the most conservative method described by Greenhouse and Geisser (1959) for unknown variance-covariance matrices. Instead of listing all simultaneous comparisons among regions, the 95% confidence limits of each region mean were computed to allow an inferential assessment of individual interregional differences. Variances were compared using a paired F test. To reduce the number of sets of regional kinetic constants for ease of future application, all compound topographic units were grouped into an optimum number of homogeneous classes by an iterative partitioning cluster analysis with maximum likelihood criterion (Mardia et al., 1979).

RESULTS

Figure 1 shows typical regions of interest on seven transverse PET slices of a healthy volunteer in comparison with corresponding CT images. Similar cross-sectional images were obtained from all subjects, and in all of them major topographical units could easily be outlined. Decay-corrected ^{18}F accumulation took a distinct time course in each of the selected regions, as demonstrated in Fig. 2 which shows original activity data, as well as fitted curves, in plasma and in some representative brain structures of the same individual.

Summary statistics on the fitted rate constants in 43 topographic regions are listed in Table 1. Since no significant asymmetries could be detected, data from corresponding regions of the two hemispheres were pooled. For all three k values, variation among subjects was highly significant ($p << 0.001$) and contributed in variable proportion to the overall variance. On the average, k_2 showed the least scatter both among regions (range 0.1198 min^{-1} in temporal white matter to 0.1472 min^{-1} in dentate nucleus) and, as indicated by small coefficients of variation, among pooled subregions or subjects (range 8.0% in thalamus to 19.9% in cerebral peduncle). Although interregional differences in k_2 were statistically significant ($p < 0.05$), they accounted for only 12.3% of the total variation as compared with relative variance components of 34.1 and 52.5% owing to variation among subjects and within regions, respectively. k_1, by contrast, was more varied not only among regions ($p < 0.001$; range 0.0485 min^{-1} in centrum semiovale to 0.0990 min^{-1} in primary visual cortex) but, to a lesser degree, also among subjects, with the average coefficient of variation ranging between 10.6% in vermis and 24.0% in occipital white matter. While the added variance component owing to interregional differences was 58.9%, variation among subjects contributed 24.0%, and within-region variability only 13.7% to the overall variance. The rate of transport from plasma to the tissue precursor pool was quite similar in cerebellum and supratentorial gray matter as opposed to white matter or mixed regions. The largest variation among structures, however, was found for k_3 ($p < 0.005$; range 0.0386 min^{-1} in temporal white matter to 0.0822 min^{-1} in caudate nucleus). Similarly, the average differences between corresponding regions of either hemisphere and among subjects were most marked for the latter rate constant, resulting in large coefficients of variation (range 9.1% in vermis to 43.5% in cerebral peduncle). Interregional variability of k_3 added 36.4%, variation among subjects 26.9%, and within regions 31.6% to the total variance. The phosphorylation rate constant was comparable in posterior fossa structures and in cerebral white matter.

Figure 3 shows all 22 average topographic regions in three-dimensional rate-constant space. It also illustrates the maximum likelihood grouping obtained by cluster analysis, indicating an optimum of four classes of brain regions: one with the lowest k_1 and k_3 comprising all the white matter and brainstem structures; another one with k_1 values similar to those of cerebral cortex and basal ganglia, but with rather high k_2 and low k_3 values, formed by cerebellar gray matter and hippocampal structures; a third group including the thalamus and most of the cerebral cortex; and one other, consisting of basal ganglia and the frontolateral and primary visual cortex, distinguished from the third class mainly by somewhat higher values for k_1 and k_3. Some of the metric similarities within each cluster may not be

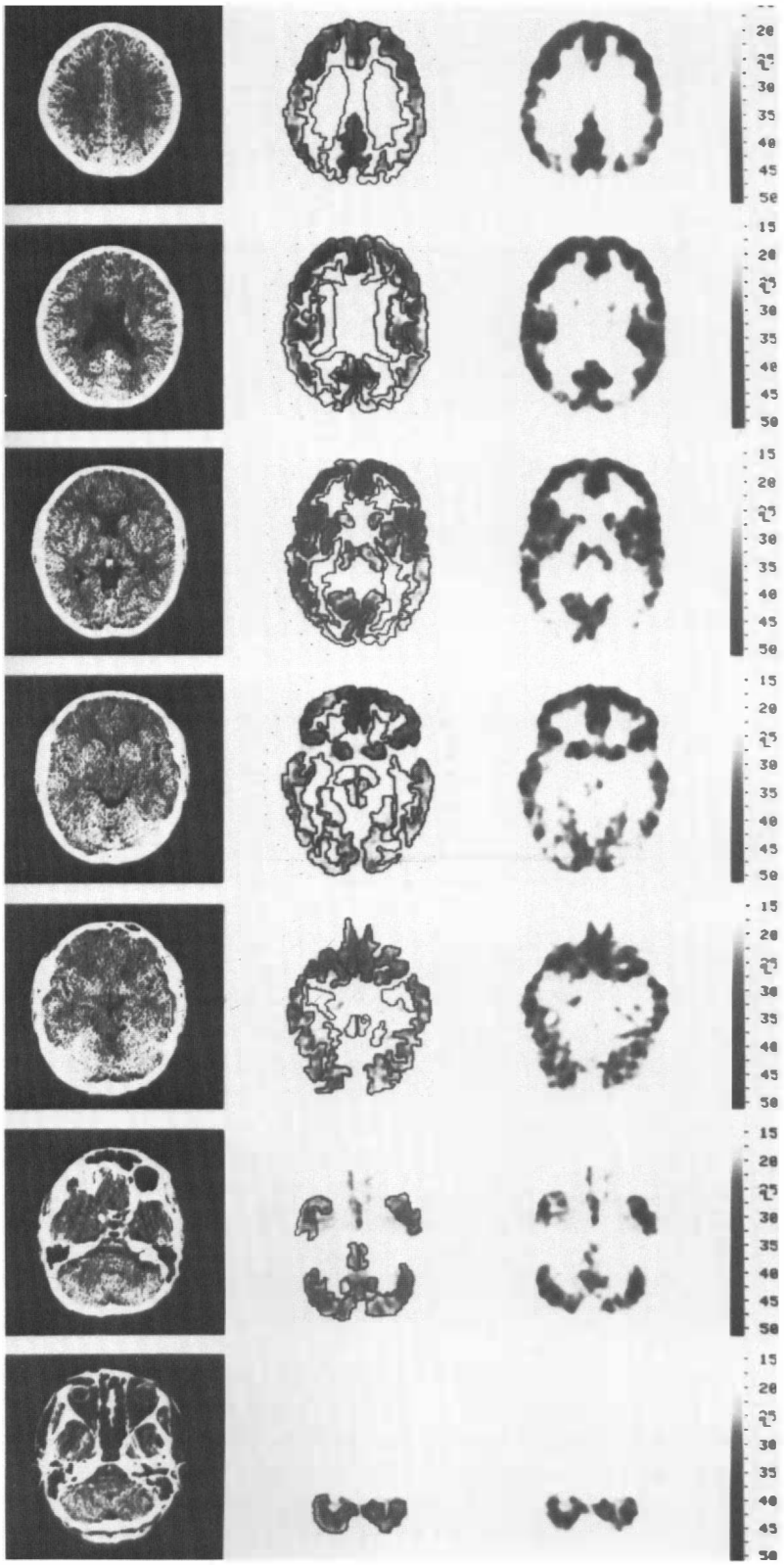

FIG. 1. X-ray computerized tomographic (left column) and corresponding [^{18}F]-2-fluoro-2-deoxy-D-glucose positron emission tomographic (right column) images of seven equally spaced transaxial sections across the brain of a 35-year-old healthy male volunteer, from the canthomeatal line (bottom row) up to 81 mm above it (top row). Center column shows contours of all regions of interest superimposed on activity maps. Reference gray scales on metabolic maps indicate local cerebral metabolic rate for glucose according to *in vivo* autoradiographic model in μmol/100 g/min.

TABLE 1. *Regional rate constants of Sokoloff model[a] in normal human subjects*

Region (n)	Side	k_1 Mean ± SD (min^{-1})	k_1 Mean of both sides (min^{-1})	k_1 95% CL of mean (min^{-1})	k_1 Av. CV (%)	k_1 Av. difference between sides (mean ± SD) (% of larger value)	k_2 Mean ± SD (min^{-1})	k_2 Mean of both sides (min^{-1})
Cerebellar cortex (30)	R	0.0911 ± 0.01313	0.0906	0.0859–0.0954	14.1	3.4 ± 2.72	0.1421 ± 0.01375	0.1418
	L	0.0902 ± 0.01292					0.1416 ± 0.1277	
Dentate nucleus (23)	R	0.0896 ± 0.02108	0.0901	0.0825–0.0977	19.5	8.8 ± 5.60	0.1462 ± 0.02204	0.1472
	L	0.0906 ± 0.01467					0.1481 ± 0.01472	
Vermis (11)	M	0.0939 ± 0.01000	0.0939	0.0872–0.1006	10.6		0.1423 ± 0.01583	0.1423
Pons (18)	R	0.0674 ± 0.01177	0.0653	0.0599–0.0706	16.4	10.6 ± 6.85	0.1329 ± 0.02859	0.1312
	L	0.0631 ± 0.00976					0.1295 ± 0.01403	
Midbrain (24)	R	0.0711 ± 0.01024	0.0729	0.0688–0.0770	13.4	8.6 ± 4.82	0.1370 ± 0.01989	0.1412
	L	0.0746 ± 0.00937					0.1454 ± 0.02031	
Cerebral peduncle (14)	R	0.0671 ± 0.01083	0.0667	0.0608–0.0725	13.8	5.4 ± 4.36	0.1481 ± 0.02958	0.1351
	L	0.0662 ± 0.00830					0.1220 ± 0.01765	
Thalamus (14)	R	0.0905 ± 0.01131	0.0886	0.0828–0.0944	11.4	5.0 ± 2.76	0.1338 ± 0.01272	0.1329
	L	0.0867 ± 0.00923					0.1321 ± 0.00901	
Lentiform nucleus (22)	R	0.0953 ± 0.01989	0.0917	0.0837–0.0997	19.7	7.6 ± 5.30	0.1423 ± 0.01709	0.1382
	L	0.0881 ± 0.01616					0.1341 ± 0.01102	
Caudate nucleus (23)	R	0.0896 ± 0.01497	0.0880	0.0814–0.0946	17.4	6.0 ± 4.36	0.1378 ± 0.01996	0.1378
	L	0.0865 ± 0.01606					0.1379 ± 0.02406	
Frontal white matter (48)	R	0.0526 ± 0.01218	0.0527	0.0491–0.0562	23.1	8.4 ± 6.05	0.1202 ± 0.01838	0.1213
	L	0.0528 ± 0.01243					0.1223 ± 0.01652	
Temporal white matter (20)	R	0.0577 ± 0.01137	0.0590	0.0542–0.0638	17.5	9.4 ± 7.13	0.1171 ± 0.01439	0.1198
	L	0.0603 ± 0.00954					0.1225 ± 0.01651	
Occipital white matter (26)	R	0.0556 ± 0.01285	0.0544	0.0491–0.0597	24.0	9.3 ± 6.17	0.1274 ± 0.01931	0.1271
	L	0.0532 ± 0.01363					0.1268 ± 0.01473	
Oval center (24)	R	0.0491 ± 0.00771	0.0485	0.0452–0.0518	16.0	5.7 ± 4.18	0.1284 ± 0.01509	0.1251
	L	0.0479 ± 0.00815					0.1219 ± 0.01176	
Cingulate gyrus (38)	R	0.0953 ± 0.01295	0.0971	0.0936–0.1006	11.1	7.2 ± 7.16	0.1359 ± 0.01584	0.1366
	L	0.0989 ± 0.00801					0.1373 ± 0.01485	
Hippocampal structures (28)	R	0.0825 ± 0.01314	0.0833	0.0781–0.0884	15.9	6.2 ± 4.08	0.1434 ± 0.01075	0.1457
	L	0.0840 ± 0.01374					0.1480 ± 0.02514	
Frontomesial cortex (72)	R	0.0937 ± 0.01080	0.0923	0.0895–0.0951	12.7	5.4 ± 4.26	0.1407 ± 0.01326	0.1381
	L	0.0909 ± 0.01261					0.1355 ± 0.01408	
Frontolateral cortex (66)	R	0.0912 ± 0.01160	0.0901	0.0874–0.0928	12.1	5.2 ± 3.22	0.1376 ± 0.01348	0.1368
	L	0.0890 ± 0.01024					0.1359 ± 0.01155	
Insular cortex (30)	R	0.0905 ± 0.01102	0.0900	0.0860–0.0941	12.0	4.2 ± 3.49	0.1383 ± 0.01287	0.1380
	L	0.0895 ± 0.01096					0.1376 ± 0.01327	
Temporal cortex (52)	R	0.0831 ± 0.01024	0.0828	0.0801–0.0856	11.9	4.7 ± 3.79	0.1350 ± 0.01255	0.1356
	L	0.0826 ± 0.00962					0.1361 ± 0.01118	
Parietal cortex (32)	R	0.0867 ± 0.00934	0.0864	0.0830–0.0898	11.0	3.6 ± 2.55	0.1363 ± 0.01294	0.1378
	L	0.0862 ± 0.00994					0.1393 ± 0.01237	
Occipital cortex (58)	R	0.0827 ± 0.01356	0.0827	0.0792–0.0863	16.2	6.7 ± 5.96	0.1407 ± 0.01445	0.1405
	L	0.0828 ± 0.01351					0.1403 ± 0.01093	
Primary visual cortex (35)	R	0.0979 ± 0.01373	0.0990	0.0943–0.1036	13.6	7.6 ± 6.59	0.1405 ± 0.01479	0.1407
	L	0.1000 ± 0.01354					0.1409 ± 0.01663	

[a] Sokoloff et al. (1977).
CL, confidence limits; CV, coefficient of variation.

TABLE 1—(*Continued*)

		k_2			k_3				
Region (n)	Side	95% CL of mean (min^{-1})	Av. CV (%)	Av. difference between sides (mean ± SD) (% of larger value)	Mean ± SD (min^{-1})	Mean of both sides (min^{-1})	95% CL of mean (min^{-1})	Av. CV (%)	Av. difference between sides (mean ± SD) (% of larger value)
Cerebellar cortex (30)	R L	0.1370–0.1467	9.2	4.4 ± 3.45	0.0468 ± 0.00547 0.0452 ± 0.00693	0.0460	0.0437–0.0483	13.5	7.6 ± 8.43
Dentate nucleus (23)	R L	0.1393–0.1551	12.3	13.5 ± 8.67	0.0519 ± 0.01335 0.0500 ± 0.01143	0.0509	0.0457–0.0562	23.8	24.1 ± 15.23
Vermis (11)	M	0.1317–0.1530	11.1		0.0414 ± 0.00377	0.0414	0.0388–0.0439	9.1	
Pons (18)	R L	0.1203–0.1421	16.7	15.3 ± 13.43	0.0490 ± 0.01438 0.0475 ± 0.01473	0.0483	0.0412–0.0553	29.3	32.7 ± 9.99
Midbrain (24)	R L	0.1327–0.1497	14.3	15.6 ± 7.44	0.0561 ± 0.02022 0.0530 ± 0.01064	0.0545	0.0478–0.0612	29.1	26.2 ± 12.02
Cerebral peduncle (14)	R L	0.1180–0.1522	19.9	18.5 ± 17.32	0.0487 ± 0.02198 0.0332 ± 0.00831	0.0409	0.0296–0.0522	43.5	27.2 ± 22.96
Thalamus (14)	R L	0.1268–0.1391	8.0	5.5 ± 4.40	0.0624 ± 0.01297 0.0652 ± 0.01596	0.0638	0.0557–0.0720	22.0	13.0 ± 7.31
Lentiform nucleus (22)	R L	0.1317–0.1447	10.6	11.5 ± 10.07	0.0748 ± 0.01676 0.0755 ± 0.02475	0.0752	0.0660–0.0843	27.4	18.6 ± 14.98
Caudate nucleus (23)	R L	0.1285–0.1472	15.7	12.2 ± 12.27	0.0837 ± 0.02490 0.0808 ± 0.02732	0.0822	0.0711–0.0933	31.2	17.1 ± 14.59
Frontal white matter (48)	R L	0.1162–0.1263	14.3	12.4 ± 9.60	0.0503 ± 0.01699 0.0512 ± 0.01906	0.0508	0.0456–0.0560	35.2	25.3 ± 18.39
Temporal white matter (20)	R L	0.1126–0.1270	12.8	9.5 ± 6.54	0.0406 ± 0.02007 0.0367 ± 0.00725	0.0386	0.0317–0.0456	38.4	30.3 ± 13.88
Occipital white matter (26)	R L	0.1203–0.1339	13.2	12.3 ± 6.50	0.0417 ± 0.01194 0.0454 ± 0.01522	0.0436	0.0381 ± 0.0490	31.1	23.9 ± 15.71
Oval center (24)	R L	0.1194–0.1309	10.9	7.6 ± 6.50	0.0512 ± 0.01440 0.0496 ± 0.01025	0.0504	0.0453–0.0556	24.3	12.0 ± 10.32
Cingulate gyrus (38)	R L	0.1316–0.1416	11.1	7.3 ± 5.89	0.0701 ± 0.01570 0.0668 ± 0.01403	0.0685	0.0636–0.0733	21.6	12.3 ± 8.00
Hippocampal structures (28)	R L	0.1382–0.1531	13.1	8.6 ± 10.10	0.0597 ± 0.02531 0.0559 ± 0.01540	0.0578	0.0498–0.0658	35.7	16.8 ± 13.08
Frontomesial cortex (72)	R L	0.1348–0.1413	10.0	7.7 ± 6.29	0.0707 ± 0.01943 0.0711 ± 0.01575	0.0709	0.0668–0.0750	24.8	15.1 ± 9.90
Frontolateral cortex (66)	R L	0.1337–0.1399	9.1	5.3 ± 5.63	0.0769 ± 0.01582 0.0756 ± 0.01789	0.0763	0.0721–0.0804	22.0	8.8 ± 6.47
Insular cortex (30)	R L	0.1333–0.1427	9.3	5.1 ± 3.56	0.0711 ± 0.01681 0.0743 ± 0.01901	0.0727	0.0661–0.0793	24.3	12.7 ± 8.27
Temporal cortex (52)	R L	0.1323–0.1389	8.7	5.9 ± 4.85	0.0668 ± 0.01537 0.0654 ± 0.01607	0.0661	0.0618–0.0704	23.6	11.9 ± 7.77
Parietal cortex (32)	R L	0.1333–0.1423	9.1	6.0 ± 4.26	0.0715 ± 0.01255 0.0716 ± 0.01640	0.0716	0.0664–0.0767	20.1	9.4 ± 6.76
Occipital cortex (58)	R L	0.1372–0.1439	9.0	5.0 ± 4.04	0.0672 ± 0.02020 0.0649 ± 0.02130	0.0660	0.0606–0.0715	31.2	11.8 ± 8.94
Primary visual cortex (35)	R L	0.1354–0.1460	11.0	9.0 ± 7.11	0.0684 ± 0.01473 0.0613 ± 0.01286	0.0647	0.0599–0.0696	21.7	17.9 ± 11.04

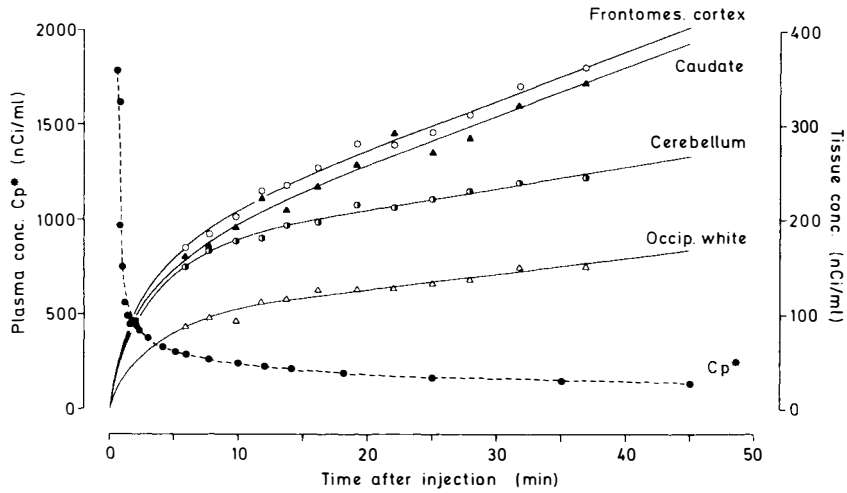

FIG. 2. Characteristic time courses of decay-corrected isotope concentrations in plasma, frontomesial cortex, caudate nucleus, cerebellar cortex, and occipital white matter of a normal volunteer. Individual symbols represent original data. Respective curves were least-squares fitted according to original three-parameter equation of Sokoloff et al. (1977).

evident from the plot, e.g., the assignment of visual cortex to the fourth group, because of lack of resolution in the k_2 dimension. The mean vectors of those four kinetic categories of topographic regions are given in Table 2.

Regional metabolic rates (CMR_{glu} kinetic) calculated according to Eq. 2 from individually fitted rate constants and pertinent statistics are presented in Table 3. Although differences between hemispheres nowhere reached any acceptable level of significance and no preference of any subject(s) for higher glucose consumption on either side could be demonstrated, variation both among individuals ($p << 0.001$) and regions ($p < 0.001$) was quite marked. Interregional differences accounted for 74.1% of the total variance as compared with 10.7% contributed by variation among subjects and 10.5% added by within-region variability. In accordance with the relation of kinetic constants described above, the lowest metabolic rates (~17 μmol/100 g/min) were found in white matter and mixed structures of the brainstem, followed by cerebellar gray matter and hippocampal structures (~28 μmol/100 g/min). All other regions exhibited greater metabolic activity, with maximum values in the cingulate and frontolateral cortex (~41 μmol/100 g/min).

As can be seen in Table 3, the metabolic rates (CMR_{glu} autoradiographic) determined according to the *in vivo* autoradiographic model showed a tendency toward higher values as compared with the kinetic approach. However, differences between the two methods with respect to their regional metabolic averages usually were small and became statistically significant in brainstem, oval center, and temporal and parietal cortex only. In all except three regions the scatter of results was significantly larger when standard rate constants were used; i.e., metabolic rates determined by the autoradiographic method were less reliable in almost any individual case. For comparison with the present results, Table 4 shows standardized estimates of regional CMR_{glu} autoradiographic and the respective coefficients of variation recalculated from data published in the literature. Because of the wide range of variation among laboratories and sometimes very small numbers of regions analyzed, particularly in the posterior fossa, comparison is difficult, but the order of regional glucose consumption as stated above still emerges as a general trend.

DISCUSSION

Rationale and methodology

The operational equation of the deoxyglucose model (Sokoloff et al., 1977) and its FDG modification (Reivich et al., 1979) was set up in such a way that influences on CMR_{glu} estimates of rate constants deviating from the norm determined for cerebral gray and white matter were minimized. Nevertheless, contrary to the findings of others (Sokoloff et al., 1977; Phelps et al., 1979), data from this study suggest that the reliability of individual rates of glucose consumption, calculated from tomographic activity maps according to the autoradiographic method, can be substantially improved by utilizing more than two standard sets of rate constants, even in normal brain tissue. Uncontrolled variability among subjects and within the same anatomical structures of the same individual is already large enough, and it is further increased by simplifying assumptions concerning kinetic constants, although the above-mentioned robustness of the metabolic model may fully apply to average values of a group of subjects because of balancing random effects. Undoubtedly the most accurate results are obtained from dynamic recordings and individually

TABLE 2. *Mean vectors of kinetic constants (min^{-1}) in maximum likelihood clusters of topographical brain regions*

Region	k_1	k_2	k_3
Pons Midbrain Cerebral peduncle Frontal white matter Temporal white matter Occipital white matter Oval center	0.0599	0.1287	0.0467
Cerebellar cortex Dentate nucleus Vermis Hippocampal structures	0.0895	0.1443	0.0490
Thalamus Cingulate gyrus Frontomesial cortex Insular cortex Temporal cortex Parietal cortex Occipital cortex	0.0886	0.1371	0.0685
Lentiform nucleus Caudate nucleus Frontolateral cortex Primary visual cortex	0.0922	0.1384	0.0746

fitted regional rate constants. This approach, however, is not only time consuming and requires a fast, highly efficient, high-resolution, multislice tomographic device with proper dead time correction and appropriate computational facilities, but in some patient studies it may not be feasible at all. Even scanning periods beyond 40 min in a fixed supine position usually are not well tolerated by neurological patients; therefore, in the present study measurements in volunteers were also restricted for the same duration. Whenever the experimental protocol or the subject examined does not permit continuous recording over prolonged periods of time, for optimum accuracy of results it would appear reasonable to use the four described sets of average rate constants. These were determined by cluster analysis as being appropriate for all brain regions, including brainstem and cerebellum, in the operational equation of the autoradiographic model.

Regional rate constants

Increased reliability of CMR_{glu} values may not be the only advantage of individually fitting regional rate constants. If the basic assumptions of the three-compartment model of FDG turnover in the brain are sound, accumulation data are not too scattered, and an advanced fit algorithm is employed, this procedure may very well yield relevant information on regional characteristics of the physiological processes described by those kinetic constants. One of the most unexpected findings of this study was the narrow range of variation, among both regions and individuals, of the rate constant representing the transport kinetics of free FDG from tissue to plasma. This observation is in contrast with data published by Phelps et al. (1979) and Huang et al. (1980), who found coefficients of variation among subjects for k_2 of 50.8 and 40.4% in cerebral gray and white matter, respectively, and by Friedland et al. (1983), who found a coefficient of variation in cerebral cortex of 31.8%. Discrepancies may be largely explained by differences in

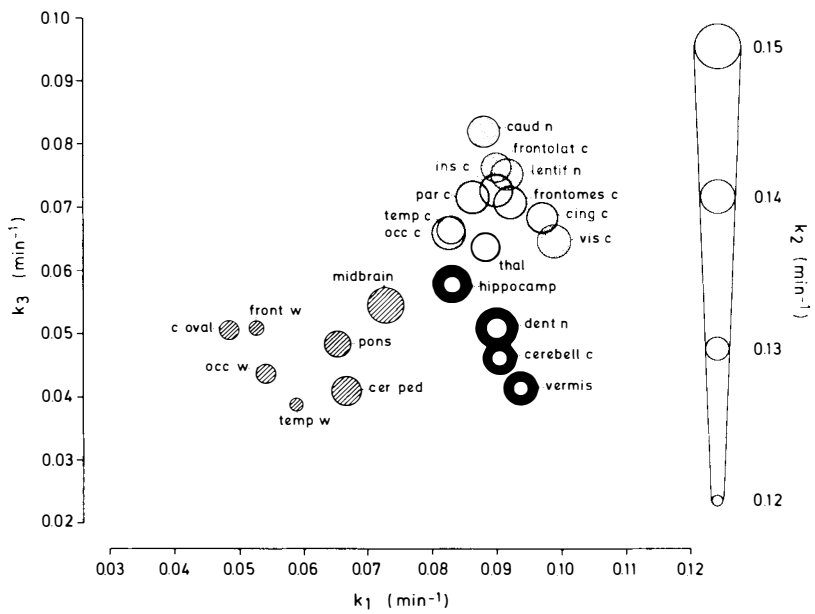

FIG. 3. Topographic brain regions of seven normal human subjects forming four distinct maximum likelihood clusters (hatched, dotted, fine-lined, and heavy-lined circles) in three-dimensional rate-constant space. Only regional mean vectors are shown.

TABLE 3. *Regional cerebral metabolic rates for glucose (CMR_{glu}) in normal human subjects—kinetic approach*

Region	Size (mean ± SD) (cm^3)	No. regions of interest evaluated	Side	CMR_{glu} kinetic (μmol/100 g/min) Either side (mean ± SD)	Both sides (mean)	95% CL of mean	Av. CV (%)	Av. difference between sides (mean ± SD) (% of larger value)	CMR_{glu} autoradiographic (mean) (μmol/100 g/min)	Av. CV (%)	Significance of differences between CMR_{glu} kinetic and CMR_{glu} autoradiographic (p value) Means	Variances
Cerebellar cortex	19.2 ± 5.74	30	R L	29.0 ± 3.88 28.2 ± 4.15	28.6	27.1–30.1	13.9	5.2 ± 5.69	28.6	19.2	(>0.1)	<0.001
Dentate nucleus	2.1 ± 1.07	23	R L	29.3 ± 4.71 29.1 ± 3.35	29.2	27.5–30.9	13.6	11.4 ± 7.96	29.0	19.8	(>0.1)	<0.002
Vermis	3.6 ± 1.66	11	M	27.6 ± 2.02	27.6	26.3–29.0	7.3		28.8	14.8	(>0.1)	<0.001
Pons	2.7 ± 0.99	18	R L	22.8 ± 4.67 21.3 ± 4.45	22.1	19.8–24.3	20.4	13.4 ± 7.10	18.8	33.8	<0.05	<0.02
Midbrain	4.3 ± 1.20	24	R L	26.0 ± 6.78 25.9 ± 5.28	26.0	23.4–28.5	22.9	13.0 ± 8.57	22.7	28.0	<0.01	(>0.1)
Cerebral peduncle	2.3 ± 0.80	14	R L	20.5 ± 4.09 17.9 ± 2.96	19.2	16.8–21.5	19.1	15.2 ± 9.25	21.4	19.5	<0.05	<0.05
Thalamus	4.0 ± 1.13	14	R L	37.0 ± 7.90 36.7 ± 7.93	36.8	32.4–41.2	20.7	5.9 ± 3.88	36.9	23.6	(>0.1)	<0.02
Lentiform nucleus	3.9 ± 1.00	22	R L	41.8 ± 7.68 39.8 ± 7.44	40.8	37.5–44.1	18.3	8.5 ± 7.37	41.6	23.5	(>0.1)	<0.005
Caudate nucleus	2.4 ± 1.19	23	R L	41.9 ± 6.65 39.9 ± 7.79	40.9	37.8–44.0	17.5	10.2 ± 6.61	40.0	20.7	(>0.1)	<0.02
Frontal white matter	14.5 ± 4.10	48	R L	19.0 ± 3.71 18.8 ± 3.03	18.9	17.9–19.9	17.7	12.1 ± 10.67	18.4	26.0	(>0.1)	<0.001
Temporal white matter	5.5 ± 2.84	20	R L	17.8 ± 4.11 17.8 ± 2.41	17.8	16.3–19.3	18.4	16.9 ± 9.60	19.2	20.5	(>0.1)	(>0.1)
Occipital white matter	15.2 ± 7.15	26	R L	16.8 ± 3.19 17.1 ± 1.51	17.0	16.0–17.9	14.4	15.7 ± 10.19	16.6	29.3	(>0.1)	≪0.001
Oval center	20.8 ± 8.15	24	R L	17.5 ± 2.65 17.4 ± 2.29	17.5	16.4–18.5	13.9	4.3 ± 3.21	15.7	19.8	<0.005	<0.01
Cingulate gyrus	10.3 ± 3.85	38	R L	40.8 ± 5.21 41.1 ± 6.03	41.0	39.2–42.8	13.6	6.0 ± 5.47	41.8	14.5	(>0.1)	<0.02
Hippocampal structures	7.3 ± 3.54	28	R L	30.1 ± 5.28 29.7 ± 5.74	29.9	27.8–32.0	18.1	8.0 ± 5.89	28.3	21.9	(>0.1)	<0.05
Frontomesial cortex	22.8 ± 3.28	72	R L	39.3 ± 5.40 39.5 ± 5.24	39.4	38.2–40.7	13.4	6.9 ± 4.56	39.6	15.8	(>0.1)	(>0.1)
Frontolateral cortex	41.4 ± 6.55	66	R L	41.6 ± 5.95 40.6 ± 5.31	41.1	39.7–42.5	13.7	3.8 ± 2.81	40.6	16.8	(>0.1)	≪0.001
Insular cortex	14.7 ± 4.05	30	R L	39.1 ± 5.61 39.8 ± 5.67	39.5	37.4–41.5	14.1	6.3 ± 4.94	39.2	17.2	(>0.1)	<0.001
Temporal cortex	32.7 ± 8.78	52	R L	35.0 ± 5.67 33.9 ± 4.72	34.4	33.0–35.8	15.1	5.6 ± 3.31	33.0	18.6	<0.05	<0.001
Parietal cortex	23.3 ± 5.88	32	R L	37.7 ± 4.05 36.6 ± 3.77	37.2	35.8–38.6	10.4	4.7 ± 3.85	36.0	12.3	<0.05	<0.05
Occipital cortex	24.3 ± 6.28	58	R L	33.5 ± 5.59 32.6 ± 5.88	33.0	31.5–34.5	17.3	6.2 ± 3.51	31.8	21.9	(=0.066)	≪0.001
Primary visual cortex	7.7 ± 2.16	35	R L	41.0 ± 5.94 39.2 ± 6.18	40.1	38.0–42.2	15.1	8.5 ± 5.91	42.6	16.8	(=0.079)	<0.001

CL, confidence limits; CV, coefficient of variation.

the fitting procedure, such as start-of-fit time and duration, particularly for the initial runs. The present results indicate a loose, albeit significant, correlation ($r = 0.56$; $p < 0.05$) between k_2 and CMR_{glu} across the entire brain, a somewhat closer correlation of k_2 with k_1 ($r = 0.79$; $p < 0.001$), but no significant association of k_2 with k_3 ($r = 0.33$; $p > 0.1$). The rate constant characterizing the kinetics of FDG transport from plasma into tissue, and to an even larger extent the rate constant for FDG phosphorylation, varied widely among regions in accordance with the functional activity and complexity of organization of the respective structures. Intersubject variation, however, was again consid-

TABLE 4. *Regional cerebral metabolic rates for glucose (CMR_{glu}) in normal human subjects. Comparison of autoradiographic CMR_{glu} values from present study with those in the literature*

	Present study	Reivich et al. (1979)	Kuhl et al. (1980)	Alavi et al. (1981)	Mazziotta et al. (1981)	Kuhl et al. (1982)	Hawkins et al. (1983)	Rapoport et al. (1983)	Rougemont et al. (1983)	Schwartz et al. (1983)
Cerebellar cortex	28.6/19.2	32.1/—			23.4/4.4					22.8/20.5
Dentate nucleus	29.0/19.8									
Vermis	28.8/14.8									
Pons	18.8/33.8									
Midbrain	22.7/28.0									
Cerebral peduncle	21.4/19.5									
Thalamus	36.9/23.6	41.2/26.0			36.6/19.2	33.4/20.9	24.3/15.2	30.7/26.2	31.5/31.5	28.4/25.0
Lentiform nucleus	41.6/23.5	35.6/7.2			45.2/20.0		36.9/22.8		38.5/14.1	33.3/14.0
Caudate nucleus	40.0/20.7	38.0/7.8	37.2/8.3		39.8/23.5	34.7/21.2	35.5/18.9	30.7/24.2	36.6/20.8	30.0/19.6
Frontal white matter	18.4/26.0	20.2/49.3	23.1/24.0							
Temporal white matter	19.2/20.5									
Occipital white matter	16.6/29.3	23.5/15.6	19.5/16.0							
Oval center	15.7/19.8	20.6/6.5	18.2/18.0		29.0/26.2	15.5/24.6	21.9/28.3	15.2/24.3		14.8/21.4
Cingulate gyrus	41.8/14.5				43.2/27.1			36.1/21.4		34.4/21.6
Hippocampal structures	28.3/21.9	33.5/4.4						24.5/28.9		24.9/28.1
Frontomesial cortex	39.6/15.8	46.0/2.4						31.5/25.9	40.4/25.2	30.5/23.8
Frontolateral cortex	40.6/16.8	47.0/4.8	37.7/13.5	26.4/?	43.0/24.2	32.7/26.3		33.6/24.5	33.3/20.3	32.2/22.9
Insular cortex	39.2/17.2									32.5/21.5
Temporal cortex	33.0/18.6	45.1/—	38.0/6.6	28.3/?	44.1/26.0	34.2/24.2		27.9/23.2	39.2/22.3	23.5/24.7
Parietal cortex	36.0/12.3	37.9/16.9	35.7/12.9	29.1/?	43.1/22.7	33.0/24.7		31.4/23.9	42.1/16.4	30.3/21.2
Occipital cortex	31.8/21.9		35.6/14.4	22.0/?	37.1/24.4	28.7/25.7		26.6/29.2		24.1/21.1
Primary visual cortex	42.6/16.8	57.0/13.4	43.7/11.7	33.2/?	46.6/23.7	40.8/23.2		33.4/21.4	46.6/25.3	30.9/18.9

Values are means (μmol/100 g/min)/coefficient of variations (%).

erably less than that described by Phelps et al. (1979) and Huang et al. (1980) (coefficients of variation of their data: k_1, gray 27.5%, white 25.9%; k_3, gray 30.6%, white 42.2%) and by Friedland et al. (1983) (coefficients of variation in cerebral cortex: k_1, 17.1%; k_3, 29.5%). Corresponding to the density of the neuropil, microvascular bed, and level of blood flow and metabolism, both k_1 and k_3 were consistently higher in supratentorial gray compared with mixed or white matter structures. A striking disparity, however, was noted in cerebellar gray matter, where k_3 stayed within the range of white matter values while k_1 was rather high, suggesting a wide safety margin of transport systems with respect to metabolic demand at rest. Accordingly, when all analyzed brain regions are considered, k_1 and k_3 show only a poor correlation ($r = 0.59$; $p < 0.05$), whereas both rate constants appear closely correlated with CMR_{glu} (k_1, $r = 0.88$; k_3, $r = 0.90$; $p << 0.001$). Comparable correlations between glucose influx and phosphorylation were reported in rats (Cremer et al., 1981; Hawkins et al., 1983*a*). In both studies considerable differences in CMR_{glu} and glucose influx rates among various brain structures were observed. Another interesting finding is the obvious similarity in kinetic constants of gray matter structures supplied by the carotid arteries, on the one side, and by the vertebrobasilar system, on the other, e.g., hippocampal formations and cerebellum.

The mean values of regional rate constants determined in this study are in good agreement with the averages found in Phelps et al. (1979) and Huang et al. (1980) for cerebral gray ($k_1 = 0.102$, $k_2 = 0.130$, $k_3 = 0.062$ min^{-1}) and white ($k_1 = 0.054$, $k_2 = 0.109$, $k_3 = 0.045$ min^{-1}) matter in single transaxial slices across the upper level of the basal ganglia of 13 normal volunteers. Minor differences are easily explained by the fact that those authors also fitted k_4 to account for dephosphorylation during prolonged recording periods. Much higher values, however, were reported for the entire cerebral cortex by Friedland et al. (1983) ($k_1 = 0.131$, $k_2 = 0.225$, $k_3 = 0.106$ min^{-1}), who took measurements at very short scanning intervals for 45 min from a midventricular slice in five healthy, aged subjects. Using other pertinent data presented by those authors and a value of 0.42 for the lumped constant, an estimate of 54.9 μmol/100 g/min is obtained for cortical CMR_{glu}, which exceeds the range of published metabolic rates (Table 4). Discrepancies with kinetic constants determined by the [^{11}C]deoxyglucose method (Reivich et al., 1982)—much higher k_2 and somewhat higher k_3 values in gray matter and much higher k_3 and somewhat lower k_2 values in white matter compared with

FDG—may be indicative of slightly different affinities of the two glucose analogs for facilitated diffusion and for hexokinase. Of course, differences in experimental and computational procedures may also play a role. If in the curve fitting of this study a fixed k_4 of, say, 10% of the average k_3 had been used, a small compensatory increase in k_3 and an increase in regional CMR_{glu} kinetic by ~6% would have ensued. However, in view of the uncertainties as to the true value of the lumped constant in humans, which itself is partly determined by k_4 (Huang et al., 1980), any consideration of an arbitrary k_4 value appeared unwarranted.

Regional CMR_{glu}

As described by Hoffman et al. (1979), there is a direct relationship between the spatial resolution of a tomographic device and the identification of neuroanatomical structures in FDG-PET. Reported regional CMR_{glu} values in normal volunteers are summarized in Table 4. At a FWHM and slice thickness of 17 mm (Mark IV scanner), major cerebral cortical and white matter regions as well as the basal ganglia and thalamus could be distinguished in two normal volunteers, and in one case the cerebellum was also studied (Reivich et al., 1979). With an ECAT positron tomograph (in-plane FWHM 17 mm; axial 18 mm) values for supratentorial structures were obtained by Kuhl et al. (1980) in eight young male controls. Alavi et al. (1981) employed the PET III whole-body tomograph (FWHM 17 mm) to estimate metabolic rates in five cortical regions of both cerebral hemispheres of six young male and four elderly normal subjects. Using the ECAT II (FWHM 16 mm; slice thickness 18 mm), averages of CMR_{glu} in several principal areas of the cerebral cortex, basal ganglia, thalamus, corpus callosum, and oval center were determined from a comprehensive set of brain tomograms in seven normal young men (Mazziotta et al., 1981*a*). Posterior fossa values were obtained from two images only. With the same tomographic system Kuhl et al. (1982) examined 40 adult volunteers of all ages and reported somewhat lower average CMR_{glu} values in supratentorial structures, without significant differences between males and females. Employing the NeuroECAT (FWHM 8.3 mm; axial resolution 13.4 mm), Hawkins et al. (1983*b*) described metabolic findings for the basal ganglia, thalamus, and white matter in four control subjects. Other studies with the ECAT II provided confirmatory information on glucose metabolism in eight cerebral gyri, caudate nucleus, thalamus, and oval center of 40 healthy men of all ages (Rapoport et al., 1983) and on larger circular supratentorial gray matter regions of seven controls (Rougemont et al., 1983); a more detailed table of regional CMR_{glu} averages in 18 healthy male volunteers was presented by Schwartz et al. (1983). Discrepancies among the reported data most likely reflect various combinations of differences: (1) among groups of subjects as to their physiological and psychological "normal resting state"; (2) in the physical characteristics of the tomographic equipment used; and (3) in the definition of regions of interest.

As expected from theoretical considerations and simulation studies (Mazziotta et al., 1981*b*), the improved spatial resolution (FWHM 7–8 mm; actual slice thickness 11 mm) of our multislice PET system (Eriksson et al., 1982) permitted assessment of CMR_{glu} in a considerable number of central nervous system structures with acceptable partial volume errors. According to the error diagrams of Mazziotta et al. (1981*b*), in the cortex (which, owing to its thickness of 2–4.5 mm, cannot be resolved without significant partial volume effects by any PET system presently in operation) regional CMR_{glu} was underestimated by 8–35%, whereas estimates for large deep circular structures (e.g., thalamus and basal ganglia) might be too low by 6–18%. Because of additional shape effects and especially unfavorable structure-to-voxel volume ratios, the most severe underestimation probably occurred in irregular posterior and basal gray matter regions. White matter structures, by contrast, suffered an overestimation of CMR_{glu} by ~10–30% owing to partial volume influences of adjacent gray matter and, to a lesser degree, underestimation by partial volume effects from cerebrospinal fluid space. All those errors, however, were considerably smaller in the data from this study than in other reported results; therefore, the improved spatial resolution is also reflected in a higher gray-to-white matter ratio of CMR_{glu} (~2.5) compared with previous observations (Table 4).

Despite all the physical limitations still inherent even in an advanced PET system, the regional CMR_{glu} in normal subjects could be determined reliably for several important structures in addition to those measured previously. Of particular interest are the normal values for formations in the posterior fossa, which differ from supratentorial structures in both morphology and function. Estimation of CMR_{glu} in these structures and their individual right/left differences also is crucial for studies of the remote effects caused by lesions in other parts of the central nervous system. Although autoradiography has a better spatial resolution (0.1 mm) and is practically unbiased by partial volume effects, variations among cerebral, cerebellar, and brain-

stem metabolic rates in humans are similar to those reported from autoradiographic studies with [^{14}C]deoxyglucose in the rat (Sokoloff et al., 1977), the cat (Ginsberg et al., 1977), and the monkey (Kennedy et al., 1978). Because of large species differences, however, absolute values cannot be compared, and so far no other method can match PET in its unique capability for providing information on temporal changes in local tracer concentrations within individuals.

REFERENCES

Alavi A, Ferris S, Wolf A, Christman D, Fowler J, MacGregor R, Farkas T, Greenberg J, Dann R, Reivich M (1981) Determination of regional cerebral metabolism in dementia using F-18 deoxyglucose and positron emission tomography. In *Cerebral Vascular Disease, Vol 3* (Meyer JS, Lechner H, Reivich M, Ott, ED, Aranibar A, eds), Amsterdam, Excerpta Medica, pp 109–112

Barrio JR, MacDonald NS, Robinson GD, Najafi A, Cook JS, Kuhl DE (1981) Remote, semiautomated production of F-18-labeled 2-deoxy-2-fluoro-d-glucose. *J Nucl Med* 22:372–375

Bergström M, Litton J, Eriksson L, Bohm C, Blomqvist G (1982) Determination of object contour from projections for attenuation correction in cranial positron emission tomography. *J Comput Assist Tomogr* 6:365–372

Bergström M, Eriksson L, Bohm C, Blomqvist G, Litton J (1983) Correction for scattered radiation in a ring detector positron camera by integral transformation of the projections. *J Comput Assist Tomogr* 7:42–50

Cremer JE, Ray DE, Sarna GS, Cunningham VJ (1981) A study of the kinetic behaviour of glucose based on simultaneous estimates of influx and phosphorylation in brain regions of rats in different physiological states. *Brain Res* 221:331–342

Eriksson L, Bohm C, Kesselberg M, Blomqvist G, Litton J, Widen L, Bergström M, Ericson K, Greitz T (1982) A four ring positron camera system for emission tomography of the brain. *IEEE Trans Nucl Sci* 29:539–543

Fowler JS, MacGregor RR, Wolf AP, Farrell AA, Karlstrom KI, Ruth TJ (1981) A shielded synthesis system for production of 2-deoxy-2([^{18}F)fluoro-D-glucose. *J Nucl Med* 22:376–380

Friedland RP, Budinger TF, Yano Y, Huesman RH, Knittel B, Derenzo StE, Koss B, Ober BA (1983) Regional cerebral metabolic alterations in Alzheimer-type dementia: kinetic studies with 18-fluorodeoxyglucose. *J Cereb Blood Flow Metabol* 3 (suppl 1):S510–S511

Ginsberg MD, Reivich M, Giandomenico A, Greenberg JH (1977) Local glucose utilization in acute focal cerebral ischemia: local dysmetabolism and diaschisis. *Neurology (Minneap)* 27:1042–1048

Greenhouse SW, Geisser S (1959) On methods in the analysis of profile data. *Psychometrika* 24:95–112

Hawkins RA, Mans AM, Davis DW, Hibbard LS, Lu DM (1983*a*) Glucose availability to individual cerebral structures is correlated to glucose metabolism. *J Neurochem* 40:1013–1018

Hawkins RA, Phelps ME, Mazziotta JC, Kuhl DE (1983*b*) A study of Wilson's disease with F-18 FDG and positron tomography. *J Cereb Blood Flow Metabol* 3(suppl 1):S498–S499

Hoffman EJ, Huang SC, Phelps ME (1979) Quantitation in positron emission computed tomography: 1. Effect of object size. *J Comput Assist Tomogr* 3:299–308

Huang SC, Phelps ME, Hoffman EJ, Sideris K, Selin CJ, Kuhl DE (1980) Noninvasive determination of local cerebral metabolic rate of glucose in man. *Am J Physiol* 238:E69–E82

Ido T, Wan CN, Fowler JS, Wolf AP (1977) Fluorination with F_2, a convenient synthesis of 2-deoxy-2-fluoro-D-glucose. *J Org Chem* 42:2341–2342

James F, Roos M (1976) MINUIT—a system for function minimization and analysis of the parameter errors and correlations. *Comput Ph* 10:343–376

Kennedy C, Sakurada O, Shinohara M, Jehle J, Sokoloff L (1978) Local cerebral glucose utilization in the normal conscious macaque monkey. *Ann Neurol* 4:293–301

Kuhl DE, Phelps ME, Kowell AP, Metter EJ, Selin C, Winter J (1980) Effects of stroke on local cerebral metabolism and perfusion: mapping by emission computed tomography of ^{18}FDG and $^{13}NH_3$. *Ann Neurol* 8:47–60

Kuhl DE, Metter EJ, Riege WH, Phelps ME (1982) Effects of human aging on patterns of local cerebral glucose utilization determined by the [^{18}F]fluorodeoxyglucose method. *J Cereb Blood Flow Metabol* 2:163–171

Mardia KV, Kent JT, Bibby JM (1979) *Multivariate Analysis.* London, Academic Press

Matsui T, Hirano A (1978) *An Atlas of the Human Brain for Computerized Tomography.* Stuttgart, Gustav Fischer Verlag

Mazziotta JC, Phelps ME, Miller J, Kuhl DE (1981*a*) Tomographic mapping of human cerebral metabolism: normal unstimulated state. *Neurology (Minneap)* 31:503–516

Mazziotta JC, Phelps ME, Plummer D, Kuhl DE (1981*b*) Quantitation in positron emission computer tomography: 5. Physical-anatomical effects. *J Comput Assist Tomogr* 5:734–743

Phelps ME, Huang SC, Hoffman EJ, Selin C, Sokoloff L, Kuhl DE (1979) Tomographic measurement of local cerebral glucose metabolic rate in humans with (F-18)2-fluoro-2-deoxy-D-glucose: validation of method. *Ann Neurol* 6:371–388

Rapoport SI, Duara R, Horwitz B, Kessler RM, Sokoloff L, Ingvar DH, Grady C, Cutler N (1983) Brain aging in 40 healthy men: rCMRglc and correlated functional activity in various brain regions in the resting state. *J Cereb Blood Flow Metabol* 3(suppl 1):S484–S485

Reivich M, Kuhl D, Wolf A, Greenberg J, Phelps ME, Ido T, Casella V, Fowler J, Hoffman EJ, Alavi A, Som P, Sokoloff L (1979) The (^{18}F)-fluorodeoxyglucose method for the measurement of local cerebral glucose utilization in man. *Circ Res* 44:127–137

Reivich M, Alavi A, Wolf A, Greenberg JH, Fowler J, Christman D, MacGregor R, Jones SC, London J, Shiue C, Yonekura Y (1982) Use of 2-deoxy-D-[1-^{11}C]glucose for the determination of local cerebral glucose metabolism in humans: variation within and between subjects. *J Cereb Blood Flow Metabol* 2:307–319

Rougemont D, Baron JC, Collard P, Bustany P, Comar D, Agid Y (1983) Local cerebral metabolic rate of glucose (lCMRG1c) in treated and untreated patients with Parkinson's disease. *J Cereb Blood Flow Metabol* 3(suppl 1):S504–S505

Schwartz M, Duara R, Haxby J, Grady C, White BJ, Kessler RM, Kay AD, Cutler NR, Rapoport SI (1983) Down's syndrome in adults: brain metabolism. *Science* 221:781–783

Sokoloff L, Reivich M, Kennedy C, Des Rosiers MH, Patlak CS, Pettigrew KD, Sakurada O, Shinohara M (1977) The [^{14}C]deoxyglucose method for the measurement of local cerebral glucose utilization: theory, procedure, and normal values in the conscious and anesthetized albino rat. *J Neurochem* 28:897–916